Structure and Speciation in Hydrous Silica Melts. 1. Temperature and Composition Effects

Kelly E. Anderson,[†] Marc M. Hirschmann,[‡] and J. Ilja Siepmann*,[†]

Departments of Chemistry and of Chemical Engineering and Materials Science, University of Minnesota, 207 Pleasant Street SE, Minneapolis, Minnesota 55455-0431, and Department of Geology and Geophysics, University of Minnesota, 310 Pillsbury Drive SE, Minneapolis, Minnesota 55455-0219

Received: March 14, 2008; Revised Manuscript Received: July 22, 2008

Monte Carlo simulations were used to investigate the phase behavior of hydrated liquid silica as a function of temperature and overall water mole fraction, x_w. Simulations using the Feuston−Garofalini potential were performed in the isobaric−isothermal ensemble at $p = 1$ GPa for 15 temperatures ($2000 \leq T \leq 9000$ K) and 25 compositions ($0.0 \leq x_w \leq 0.4$). The unusual volume minimum exhibited by tetrahedrally coordinated liquid silica is found to persist up to $x_w \approx 0.267$, although the temperature of the volume minimum decreases with increasing water content. Structural properties of the pure and hydrated systems are compared and the addition of water to liquid silica disrupts the silica network more dramatically than temperature alone. The simulations yield very low concentrations of molecular water, e.g. only about 1.2% of the oxygen atoms are bound to exactly two hydrogen atoms at $x_w = 0.4$ and $T = 3000$ K.

1. Introduction

Silica (SiO_2) plays a significant role in the chemistry and mineralogy of the Earth's crust and mantle. SiO_2 accounts for more than 40 wt % of Earth's mantle and more than 50 wt % of its crust.[1] Dissolved volatiles are known to have important effects on the properties of silicate melts.[2] Water, in particular, plays an important role in many global processes and has received much attention.[3,4]

Much of what is known about hydrous silica melts comes from spectroscopic and diffraction measurements on glasses quenched from melts. Building on an earlier review by McMillan,[3] Kohn[4] presents a straightforward analysis of the techniques used to quantify the OH/H_2O ratio in hydrous melts, including the limitations of each technique. These limitations include instrument dependence, unresolved peak structures, insensitivity to certain species present in glasses or melts of interest, and the assumption that the structures seen in the glass are also relevant for the melt. Perhaps the most challenging limitation is the difficulty of performing in situ measurements under the conditions necessary to study hydrous silica melts.

In contrast, molecular simulations are not limited by temperature and pressure conditions. Instead, the crucial choice is that of the interaction potential. A potential must be able to account for the interaction of oxygen atoms in a variety of situations (SiOSi, SiOH, HOH, OH, etc.), bonds must be able to break and form, and the parameters must be relevant at the conditions of interest. While first principles techniques have the advantage of relying on electronic structure calculations to determine the interatomic forces and speciation, these simulations are very expensive and currently impractical for systems of more than a hundred atoms. Several studies have used first principles molecular dynamics to investigate primarily the structural and dynamical properties of liquid silica.[5−9] Pöhlmann et al.[10] carried out a first principles molecular dynamics simulation of a system of 102 atoms with 3.84 wt % water ($x_w = 0.118$). This is equivalent to a system of 30 SiO_2 formula units and 4 H_2O molecules. At a fixed density of 2.05 g/cm^3 and temperatures of 3000 and 3500 K, they found that after 5 ps most of the water had dissociated into SiOH groups attached to the silica network. Water molecules and free OH groups were only present at the higher temperature and did not persist over the length of the simulation.

In this study, we explored temperature effects on liquid and hydrated liquid silica using the empirical Feuston−Garofalini (FG) force field.[11,12] Few reactive silica force fields[11−16] are available for investigating silica−water interactions, i.e. those that allow Si−O and O−H bonds to break and form and new species to evolve from the starting units. The FG force field satisfies these criteria and has a straightforward form that is easy to implement. Furthermore, it has been used previously to examine the high temperature−pressure behavior of a pure silica melt.[17] This paper will proceed as follows: in section 2, we will provide the methodological details of the study; in section 3, an analysis of the simulations; and in section 4, a summary of these findings. In the companion to this paper,[18] pressure effects on hydrated silica are discussed.

2. Methods

2.1. Potential. The FG force field is comprised of two- and three-body terms,

$$U(\{\mathbf{r}\}) = \sum_{i,j} U_2(\mathbf{r}_i,\mathbf{r}_j) + \sum_{i,j,k} U_3(\mathbf{r}_i, \mathbf{r}_j, \mathbf{r}_k) \tag{1}$$

where $\{\mathbf{r}\} = (\mathbf{r}_1, \mathbf{r}_2, ..., \mathbf{r}_N)$ is the set of Cartesian coordinates for an N atom system. The two-body terms include a modified Born−Mayer−Huggins (BMH) potential to account for repulsive and Coulombic interactions and the Stillinger−Rahman (SR) potential for water[19]

$$U_2(\mathbf{r}_i, \mathbf{r}_j) = U^{\mathrm{BMH}}(r_{ij}) + \sum_k U_k^{\mathrm{SR}}(r_{ij}) \tag{2}$$

$$U^{\mathrm{BMH}}(r_{ij}) = A_{ij} \exp\left(\frac{-r_{ij}}{\rho_{ij}}\right) + \frac{q_i q_i}{r_{ij}} \operatorname{erfc}\left(\frac{r_{ij}}{\beta_{ij}}\right) \tag{3}$$

* Corresponding author. E-mail: siepmann@umn.edu.
[†] Departments of Chemistry and of Chemical Engineering and Materials Science.
[‡] Department of Geology and Geophysics.

10.1021/jp802253d CCC: $40.75
Published on Web 09/24/2008

$$U_k^{SR}(r_{ij}) = \frac{a_{ij}^{(k)}}{1 + \exp[r_{ij} - c_{ij}^{(k)}]} \quad (4)$$

where r_{ij}, q_i, and q_j are the separation and partial charges for the atoms i and j. For most interactions, U_k^{SR} is zero, but for those involving a hydrogen atom, U_k^{SR} is included to increase structure.[11,12] Differing X−H interactions require different numbers of contributions to U_2, such that k ranges from 1 to 3. The FG modification to the BMH potential form is applied to the Coulombic term. Instead of using a long-range potential form, requiring an Ewald sum, a short-range screening term is applied to the Coulombic interactions. This allows the charge interactions between atoms to be considered over a short separation distance. Screening effects and incomplete charge transfer are treated empirically by the size-independent, species-dependent adjustable term, β_{ij}.[20] These interactions were truncated at 5.5 Å in vitreous silica, where short-range interactions are sufficient to model the important features.[11] For the liquid, a longer cutoff of 6.5 Å was used to minimize the shift necessary to bring the potential for each interaction to zero at the cutoff. The SR term accommodates the exchange of oxygen atoms between water, hydroxide, and the silica network. In particular, this term influences the hydrogen interactions with the other atoms in the system.

The three-body terms were introduced for Si−O−Si and O−Si−O angles to impose order on nearest neighbor geometries in the system.[11,12]

$$U_3(\mathbf{r}_i, \mathbf{r}_j, \mathbf{r}_k) = v_3(r_{ij}, r_{ik}, \theta_{jik}) + v_3(r_{jk}, r_{ji}, \theta_{kji}) + v_3(r_{ki}, r_{kj}, \theta_{ikj}) \quad (5)$$

$$u_3(r_{ij}, r_{ik}, \theta_{jik}) = \begin{cases} \lambda_{jik}\left[\exp\left(\frac{\gamma_{ij}}{r_{ij} - r_{ik}^{\circ}} + \frac{\gamma_{ik}}{r_{ik} - r_{ik}^{\circ}}\right)\right](\cos\theta_{jik} - \cos\theta_{ijk}^{\circ})^2 & \text{for } r_{ij} < r_{ij}^{\circ} \text{ and } r_{ik} < r_{ik}^{\circ} \\ 0 & \text{otherwise} \end{cases} \quad (6)$$

When θ_{jik} varies from the specified angle θ_{jik}°, this term acts as a penalty function to increase the system energy. The form is taken from the effective potential for silicon developed by Stillinger and Weber.[21]

2.2. Simulation details. Monte Carlo (MC) simulations were carried out in the isobaric−isothermal ensemble,[22] using atomic translation moves and volume changes to sample phase space. Periodic boundary conditions were imposed to mimic a bulk system. All simulations were carried out at 1 GPa and over a temperature range of 2000−9000 K. This is well above the experimental melting point of silica (β-quartz: 1900 ± 20 K at 1 GPa[23]). Each simulation system was composed of 60 formula units (180 atoms). This number was held constant as the ratio of water molecules to silica formula units in the initial setup of the system was increased one-by-one from 0 water molecules (60 silica formula units) to 24 water molecules (36 silica formula units). This gives a range of overall water mole fractions, x_w, from 0 to 0.4. The following discussion will focus chiefly on 5 compositions: the pure silica system referred to as 0W and the systems with $x_w = 0.1$, 0.2, 0.3, and 0.4 (10W, 20W, 30W, and 40W, respectively).

Each system was heated initially to 6000 K and allowed to equilibrate (monitoring for convergence of the internal energy, density, and various coordination numbers). For the four highest temperatures, 4500, 6000, 7500, and 9000 K, each simulation was fully equilibrated at the specified temperature from the final configuration of the 6000 K simulation and ensemble averages were collected over 3×10^6 MC cycles, where one cycle consists of $N = 180$ moves. The final configuration of the 4500 K simulation was cooled to 3000 K and equilibrated, followed by the production simulation (3×10^6 MC cycles). The simulations at 2000−2900 K were performed by cooling stepwise from the final configuration of the next highest temperature in 100 K steps (using 10^6 MC cycles for equilibration and 3×10^6 for production).

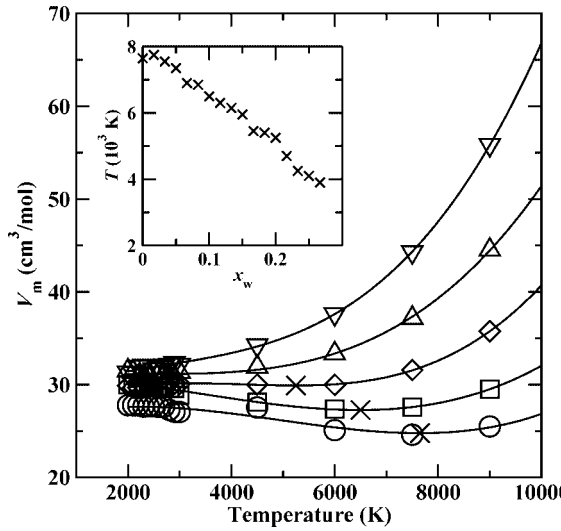

Figure 1. Molar volume versus temperature for selected compositions (main graph) and temperature of the volume minimum (inset). Circles, squares, diamonds, triangles up, and triangles down refer to systems 0W, 10W, 20W, 30W, and 40W, respectively. The lines show a third-order polynomial fit to the data. For those fits with a minimum falling into the temperature interval investigated here, the cross indicates the position of the volume minimum. All error bars are smaller than the symbol size. The inset shows the composition dependence of the temperature of the volume minimum.

Five independent sets of simulations were run for each composition and temperature, starting from different initial densities. All results are averaged over these five sets of simulations. Unless otherwise noted, error bars indicate the standard error of the mean determined from these independent simulations.

3. Results and Discussion

3.1. Molar Volume. Figure 1 shows volume−temperature curves for selected compositions over the range of temperatures simulated here. Different behavior is evident for the low and high water concentration systems. For the 0W and 10W systems, V_m passes through a minimum at 7650 and 6500 K, respectively, as indicated by the polynomial fit. For systems 20W and 30W, V_m remains fairly constant until approximately 4500 K, after which it steadily increases with temperature. For the highest water concentration, system 40W, V_m already is seen to increase by about 3% in the temperature interval from 2000−3000 K.

Experimental measurements by Brückner show a minimum near 1800 K in the volume−temperature curve for undercooled melts of vitreous silica with low hydroxyl content, but this anomalous behavior disappears for hydroxyl-rich silica glasses.[24] Clearly, the FG force field significantly overestimates the temperature of the volume minimum, but reproduces the behavior that the minimum vanishes for higher hydroxyl (total water) content. Recently, Karki et al.[9] performed a large number of first principles simulations for pure silica using the local density approximation and found a very small temperature dependence of the molar volume at low pressure, but not a volume minimum in the temperature range from 3000 to 6000

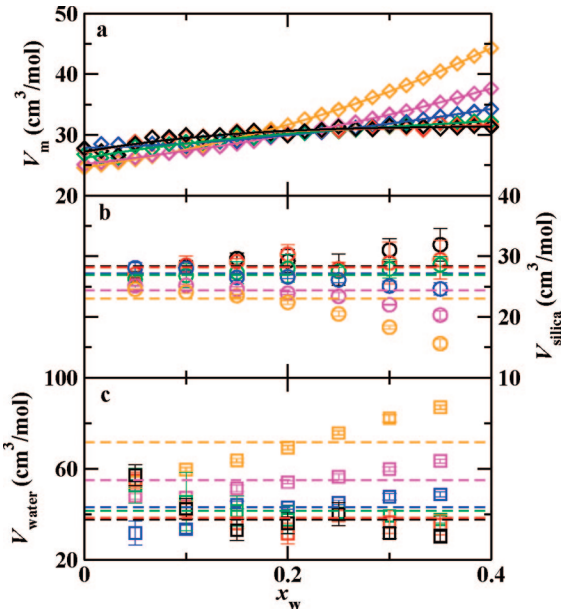

Figure 2. Molar volume versus composition for selected temperatures. (a) Total molar volume. Solid lines indicate a third-order polynomial fit to the data. (b) Partial molar volume of silica. (c) Partial molar volume of water. Symbols and dashed horizontal lines denote fits using composition-dependent and composition-independent partial molar volumes, respectively. Black, red, bright green, blue, magenta, and orange correspond to 2000, 2500, 3000, 4500, 6000, and 7500 K, respectively. Error bars indicate an 80% confidence interval over the results from five simulations.

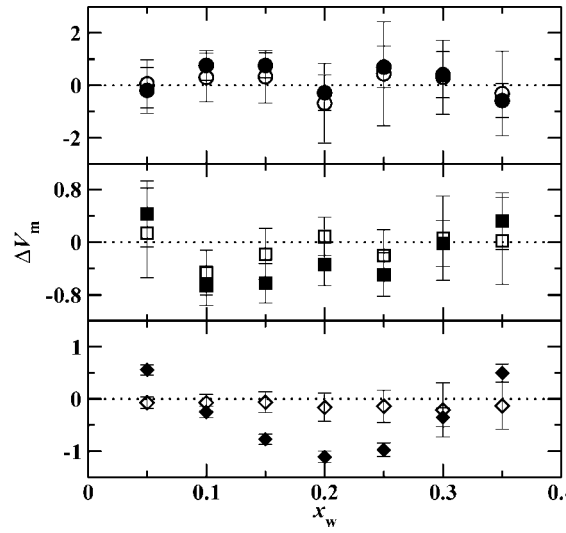

Figure 3. Residual errors obtained from least-squares fits of the molar volume using composition-dependent (open symbols) and composition-independent (filled symbols) partial molar volumes at 2000 (top), 4500 (middle), and 7500 K (bottom). Error bars indicate an 80% confidence interval over the results from five simulations.

K. In previous molecular dynamics simulations for the FG force field carried out by Kuzuu et al.,[17] the volume−temperature curve remained linear up to 5200 K where the slope of the curve became negative and a volume minimum occurred at 7600 K, i.e. in good agreement with the temperature of the volume minimum found here. Our simulations indicate that the temperature of the volume minimum is lowered by about 1200 K with each addition of 0.1 mol fraction of water, but the extent of the volume minimum gradually lessens with increasing water concentration and no volume minimum is found for $x_w > 0.267$ (Figure 1, inset).

3.2. Partial Molar Volume. Figure 2a shows isotherms of the system molar volume as a function of the overall mole fraction of water. For the isotherms at $T \leq 3000$ K, there is considerable scatter in the data, but it is clear that all isotherms show significant curvature. Given the nonlinearity of the volume−composition isotherms, the partial molar volumes, $\bar{V}$, of silica and water were determined by a least-squares fit to the equation

$$V_m(x_w) = x_w \bar{V}_{water}(x_w) + (1 - x_w)\bar{V}_{silica}(x_w) \qquad (7)$$

where V_m is the ensemble average of the system molar volume (computed assuming molecular species). This equation was fit using the 6 compositions surrounding a given value of x_w, i.e. simulations with 3−9 water molecules to determine the partial molar volumes at $x_w = 0.1$ (6 water molecules).

The partial molar volumes are depicted in Figure 2. For the low temperature simulations ($T \leq 3000$ K), the partial molar volume of silica remains fairly constant near 28 cm^3/mol, increasing slightly as the overall mole fraction of water increases. Under these conditions, the corresponding $\bar{V}_{water}$ initially decreases with increasing water content up to $x_w = 0.15$, but for higher x_w remains fairly steady at ≈34 cm^3/mol ($T =$ 2000 K) and ≈40 cm^3/mol (3000 K). In this region, the line fit to V_m versus x_w is concave down (see Figure 2a) and shows the largest curvature for small values of x_w. At higher temperatures ($T > 4500$ K), $\bar{V}_{silica}$ decreases as x_w rises above 0.1, while $\bar{V}_{water}$ increases almost linearly with water fraction to very large values. For these temperatures, the lines in Figure 2a are concave up.

Experimental data for hydrous silica are not available for the temperature and composition range investigated here. Ochs and Lange[25] analyzed several different experimental data sets for hydrous albitic ($NaAlSi_3O_8$) liquids with 1.9−6.1 wt % H_2O ($0.1 < x_w < 0.3$), temperatures from 600−1875 K and pressures up to 1 GPa. Using a multiple linear regression, the partial molar volumes of component species, including SiO_2 and H_2O, were determined.[25] In this case, the partial molar volumes are taken to be independent of water concentration. The resulting values for silica and water at $T = 1673$ K are 26.9 and 27.8 cm^3/mol, respectively.[25]

For comparison, the simulation data for the FG potential were also fit using composition-independent partial molar volumes, that is $V_m(x_w) = x_w \bar{V}_{water}^\circ + (1 - x_w)\bar{V}_{silica}^\circ$ (see Figure 2). At 2000 K, the resulting composition-independent partial molar volume, $\bar{V}^\circ$, of silica is 28.3 ± 0.2 cm^3/mol and $\bar{V}_{water}^\circ$ is 37.7 ± 0.7 cm^3/mol. $\bar{V}_{silica}^\circ$ is in fairly good agreement with the experimental value (considering the higher temperature used in the simulations), but $\bar{V}_{water}^\circ$ is significantly larger than the experimental value. As can be seen in Figure 2, it is found that the composition-independent partial molar volume of silica decreases slightly with increasing temperature, whereas that of water nearly doubles when the temperature is increased from 2000 to 7500 K.

Our approach of using composition-dependent partial molar volume for water and silica (see eq 7) is in striking contrast to a wide body of experimental data for molten silicates indicating that the partial molar volumes of most oxide components are compositionally invariant.[26] However, experimental data above 2000 K are very scarce. Figure 3 shows that using composition-dependent $\bar{V}(x_w)$ yields significantly smaller residual errors at $T \geq 4500$ K than using composition-independent $\bar{V}$. The system volume at 2000 K, though, is equally well described using either composition-dependent on composition-independent $\bar{V}$. Thus, one may argue that $\bar{V}(x_w)$ are only needed for conditions more extreme than found in the Earth's mantle.

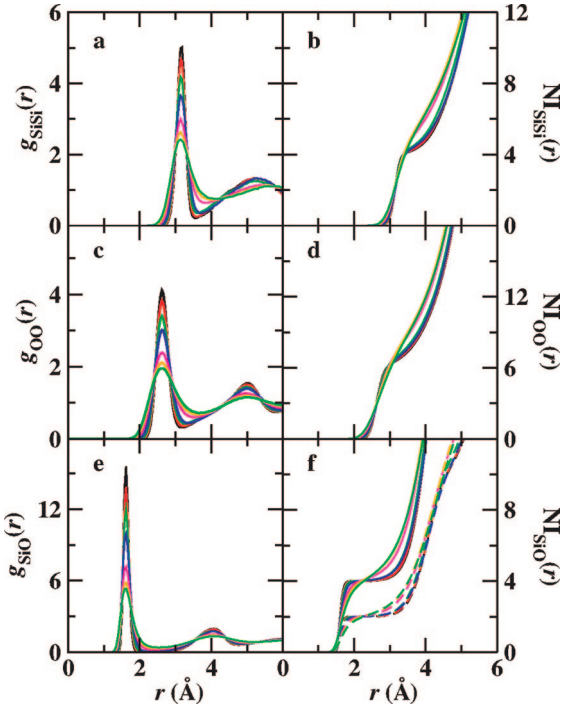

Figure 4. Radial distribution functions (left) and number integrals (right) for the 0W system. In part f, the solid and dashed lines represent the Si−O and O−Si number integrals, respectively. Black, red, bright green, blue, magenta, orange, and dark green correspond to 2000, 2500, 3000, 4500, 6000, 7500, and 9000 K, respectively.

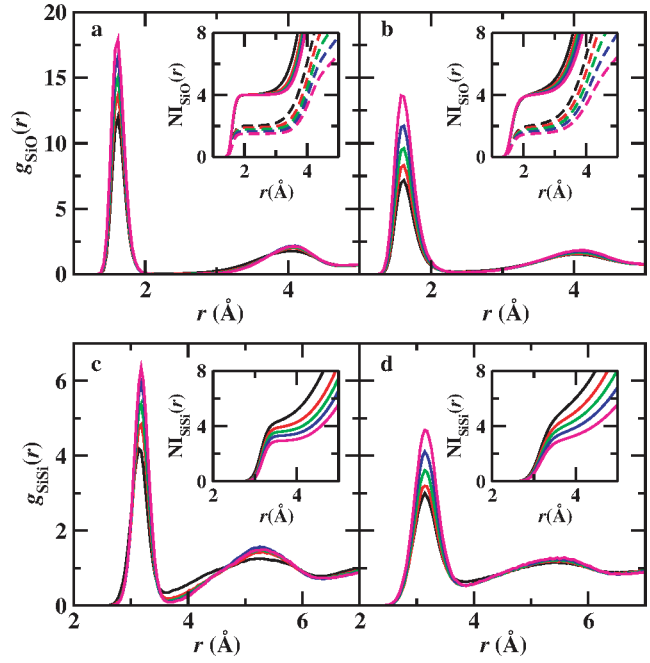

Figure 5. Radial distribution functions and number integrals (inset) for the hydrated systems. (a) Si−O RDF at 3000 K. (b) Si−O RDF at 6000 K. (c) Si−Si RDF at 3000 K. (d) Si−Si RDF at 6000 K. In the number integral insets for Si−O, solid and dashed lines indicate Si−O and O−Si NIs, respectively. Black, red, bright green, blue, and magenta correspond to 0W, 10W, 20W, 30W, and 40W, respectively.

TABLE 1: First Peak and First Minimum Distances and Coordination Number at the First Minimum Calculated from the RDFs and NIs of Pure Silica from 2000−9000 K[a]

	Si−Si			O−O			Si−O			
temp	r_P	r_M	CN	r_P	r_M	CN	r_P	r_M	CN_{SiO}	CN_{OSi}
2000	3.18	3.54	4.16	2.62	3.18	6.61	1.62	2.14	4.00	2.00
2500	3.14	3.58	4.22	2.62	3.22	6.74	1.62	2.14	4.00	2.00
3000	3.14	3.58	4.38	2.62	3.26	7.10	1.62	2.26	4.02	2.01
4500	3.14	3.70	4.47	2.62	3.30	7.04	1.62	2.34	4.03	2.02
6000	3.14	3.86	5.59	2.62	3.50	8.69	1.62	2.38	4.15	2.08
7500	3.14	3.98	6.34	2.62	3.62	9.34	1.62	2.42	4.25	2.12
9000	3.14	4.18	7.00	2.62	3.70	9.92	1.62	2.50	4.34	2.17

[a] For Si−O, both SiO and OSi coordination numbers are provided.

3.3. Distribution Functions. The atom−atom radial distribution functions (RDFs) and number integrals (NIs) for the pure silica system are shown in Figure 4 as a function of temperature. A bin width of 0.04 Å was used for all RDFs. The positions of the first peak and first minimum, and the corresponding coordination number(s), are given in Table 1. In each RDF, the position of the first peak does not change as the temperature increases, but the height of that peak decreases with increasing temperature. In the Si−Si and O−O RDFs (Figures 4a and c), the overall shape and width of the peaks remain very similar from 2000−4500 K. The location of the first minimum shifts by only 0.2 Å over this temperature region. Between 4500 and 6000 K, a large decrease in the first peak height occurs for both RDFs. Accompanying this decrease is a noticeable broadening of the first peak and a shift of the first minimum to larger separations. This can be seen more clearly in the NI (Figures 4b and d). The shape of the NI for each pair interaction changes dramatically between 4500 and 6000 K, increasing the self-coordination number of Si and O atoms. These effects indicate a change in structure above 4500 K, particularly a loss of (tetrahedral) long-range structure. This is the temperature region where the slope of V_m vs T is negative.

In contrast, in the Si−O RDF (Figure 4e), the peak height does not change dramatically between 4500 and 6000 K. Instead, with increasing temperature, the height decreases steadily, accompanied by slight broadening. However, the depth and shape of the first minimum changes more abruptly from a value of ≈0.05 with a square-well-type shape to ≈0.2 with a rounded shape. Correspondingly, the NI (Figure 4f) indicates a distinct change in coordination between 4500 and 6000 K. Despite this, the average coordination number at the first minimum for Si around O (N_{OSi}) and O around Si (N_{SiO}) remains near 2 and 4, respectively, for all temperatures. Si and O form very strong bonds in the silica system and a large amount of energy is necessary to distort these bonds away from a tetrahedral environment for SiO_4 fragments.

The addition of water has little effect on the coordination and structure of Si and O atoms. At 3000 and 6000 K, the Si−O RDFs for different x_w look remarkably similar (Figures 5a and b). It is important to note that as the water content of the system increases, the overall number of Si and O atoms decrease. The change in peak height with increasing water concentration seen in Figure 5 arises due to the normalization over a smaller number of Si and O atoms and not necessarily due to increasing structure, as seen in the softening of the NI as x_w increases (Figure 5 inset). As with temperature, increasing the water content does not appear to have a great effect on the Si−O coordination environment. At the first minimum of the RDF, N_{OSi} and N_{SiO} remain constant at approximately 2 and 4 for both of these temperatures and all compositions.

In contrast, the Si−Si NI changes dramatically as x_w increases. At 3000 K (Figure 5c), the coordination number for Si−Si at the minimum of the RDF is near or slightly above 4 for systems with $x_w \leq 0.2$. This is the expected value for a tetrahedral system. As the water content increases ($x_w > 0.2$), N_{SiSi}

TABLE 2: First Peak and First Minimum Distances and Coordination Number at the First Minimum Calculated from the RDF and NI of Hydrated Silica at 3000 and 6000 K[a]

	Si−Si			Si−O			
x_w	r_P	r_M	CN	r_P	r_M	CN_{SiO}	CN_{OSi}
			3000 K				
0.0	3.14	3.58	4.38	1.62	2.26	4.02	2.01
0.1	3.18	3.70	3.98	1.62	2.22	4.02	1.91
0.2	3.18	3.66	3.61	1.62	2.30	4.01	1.78
0.3	3.18	3.74	3.34	1.62	2.30	4.01	1.65
0.4	3.18	3.70	2.95	1.62	2.26	4.01	1.50
			6000 K				
0.0	3.14	3.86	5.59	1.62	2.38	4.15	2.08
0.1	3.14	3.86	4.74	1.62	2.42	4.12	1.95
0.2	3.14	3.82	4.14	1.62	2.42	4.09	1.82
0.3	3.14	3.82	3.66	1.62	2.42	4.06	1.67
0.4	3.14	3.86	3.19	1.58	2.46	4.05	1.52

[a] For Si−O, both SiO and OSi coordination numbers are provided.

decreases, to below 3 for the 40W system (Table 2). At 6000 K (Figure 5d), where systems with $x_w \leq 0.25$ are within the volume depression region, N_{SiSi} increases to as much as 5.6. The silica network has been compressed, pushing additional Si atoms into the nearest neighbor sphere. With increasing water content, where there is no volume depression (see Figure 1), the coordination number is below the tetrahedral number. While both the presence of water and increasing the temperature act to change the structure of silica, hydrating the systems leads to greater changes in the coordination environment compared to temperature effects.

This structural deformation is seen as well in the analysis of the angular distribution functions. In each plot for pure silica (Figure 6), there is a marked gap between the low temperature (≤4500 K) and high temperature (>4500 K) regions. Up to 4500 K, the angular distribution is steady with only slight broadening as the temperature increases. At higher temperatures, the broadening becomes more pronounced, both to larger and smaller angles. The first two rows of Figure 6 show angles which are subject to the penalty function in the three-body term of the FG potential (Si−O−Si and O−Si−O). This penalty function is only a small fraction of the overall energy of any given configuration of the system, but it is clearly sufficient to maintain the bond angle distribution, particularly for O−Si−O angles. The third distribution function (Figures 6c and f) is for the Si−Si−Si angle that is not a bond bending angle (since the Si atoms are separated by O atoms) and is not subject to a specific penalty. The Si−Si−Si distribution shows a more dramatic change as a function of temperature. Below 6000 K, the majority of the Si−Si−Si angles are larger than 90° with only a small number of Si−Si−Si triads found with $\theta < 90°$. As the temperature reaches and passes 6000 K, the distribution begins to level out for $\theta \geq 90°$, but a sharp increase in the number of angles with $\theta < 90°$ is seen. The interpenetration of multiple silica networks, as a result of the compression of the overall system (at 1 GPa), forces Si atoms into nearer proximity. For the 20W system (Figures 6d−f), this process is more gradual. The Si−O−Si and O−Si−O distributions steadily broaden as the temperature increases. For Si−Si−Si, the large angle peak gradually broadens to an almost even distribution at high temperatures, while the small angle peak increases with temperature.

3.4. Coordination Environments. While the NIs show the average coordination environment of a given atom, we are

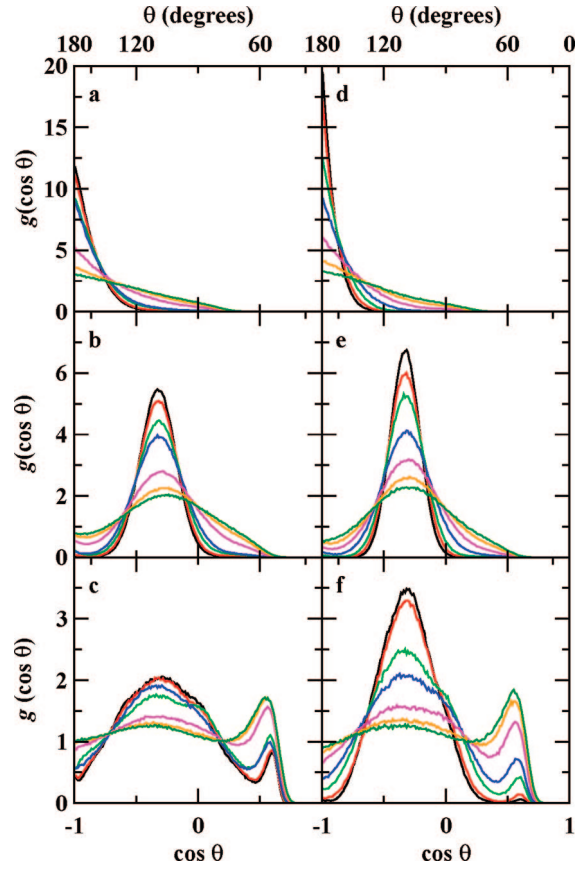

Figure 6. Angle distribution functions for the 0W (left) and 20W (right) systems. (a and d) Si−O−Si. (b and e) O−Si−O. (c and f) Si−Si−Si. Black, red, bright green, blue, magenta, orange, and dark green correspond to 2000, 2500, 3000, 4500, 6000, 7500, and 9000 K, respectively.

interested in the coordination species present as well. Figure 7 shows the fraction of Si and O atoms in different coordination environments, f_{AB_n}, where n is the number of neighboring atoms of type B around an atom of type A. Neighboring atoms are defined as those separated by a distance less than the first minimum of the RDF. In this analysis, we found the coordination number to be very sensitive to the Si−O cutoff distance. Using a cutoff of 2.2 Å, which was used by Kuzuu et al.,[10] f_{SiO_3} doubles at 6000 K to 0.071 from 0.035 and f_{SiO_4} increases slightly (from 0.82 to 0.85) while f_{SiO_5} is nearly halved (from 0.14 to 0.083). In contrast, increasing the cutoff to 2.5 Å reverses this trend. Tetrahedral and undercoordination decrease to 0.75 and 0.018, respectively, while overcoordination increases to 0.22. There is also a rise in contributions from larger values of n. A cutoff of 2.35 Å, i.e. near the first minimum in the RDF at 4500 K for 0W, was chosen as an intermediate value to facilitate comparison between both different temperatures and different compositions.

In the 0W system, the majority of Si atoms are surrounded by four O atoms (Figure 7a). At low temperatures, more than 95% of Si atoms are in a tetrahedral environment. As the temperature increases, f_{SiO_4} decreases and f_{SiO_5} increases. The contraction of the network as the temperature increases allows for this overcoordination of the Si atoms. The undercoordinated species, Si atoms bound to three O atoms, account for only a small number of the Si atoms even at high temperatures. Similarly, the majority of the O atoms in pure silica have two Si nearest neighbors (Figure 7c). As the temperature increases and the volume contracts, f_{OSi_2} decreases slightly and f_{OSi_3}

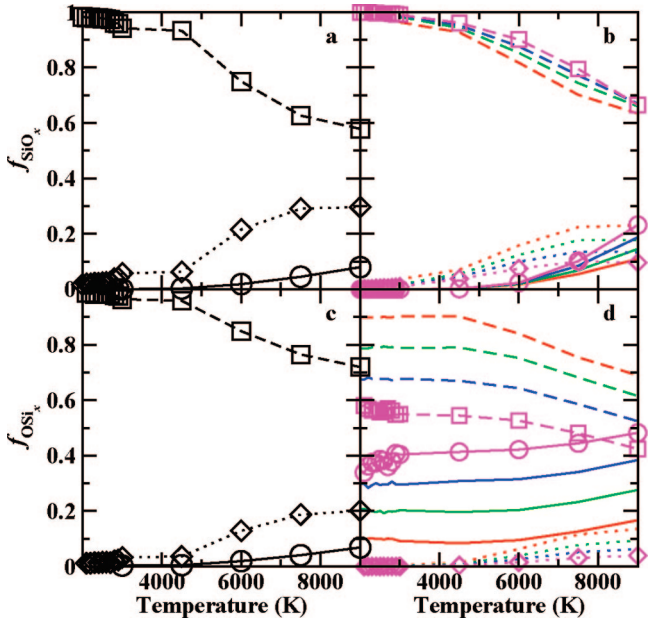

Figure 7. Coordination environments as a function of temperature. Plots a and b show oxygen coordination around silicon; plots c and d, silicon around oxygen. Squares (dashed), circles (solid), and diamonds (dotted) represent tetrahedral coordination (SiO_4/OSi_2), undercoordination (SiO_3/OSi_1), and overcoordination (SiO_5/OSi_3), respectively. The 0W system is on the left, while 10W (red), 20W (blue), 30W (green), and 40W (magenta) are on the right. Lines are provided as a guide for the eye. For the hydrated systems (b and d) symbols are only shown for 40W for clarity.

increases. At every temperature, the majority of the atoms are found in a tetrahedral coordination environment in 0W. This trend is consistent with the first principles simulations of Pöhlmann et al.,[10] where it was found that at 3500 K, 7% of Si atoms have 5-fold coordination and 4% have 3-fold, while at 3000 K these numbers are 2% and 1%, respectively. In contrast, the trend toward overcoordination is opposite of the trend found in the MD simulations of Kuzuu et al.[17] They see little evidence of overcoordination of either Si or O, but a large increase in undercoordination with increasing temperature for both atoms. As noted above, Kuzuu et al. used a distance cutoff that is 0.15 Å shorter than that used here. We find that using this shorter cutoff distance, it is possible to increase undercoordination and decrease overcoordination, although not to the extent seen in ref 17.

The right side of Figure 7 shows the trends in coordination number with changing liquid composition. Comparing Figure 7a and b, the Si environments in the hydrated system appear to be very similar to the pure system. At all temperatures and for all compositions the majority of Si atoms are surrounded by four O neighbors. The Si−O bond is very strong, as seen in the radial distribution function. More than 60% of the Si atoms retain a local tetrahedral environment under all the conditions examined here. For the hydrated systems, as the temperature and overall mole fraction of water increase, f_{SiO_3} increases. This is consistent with the NIs in Figure 5.

The local environments of the O atoms in the hydrated systems show greater differences relative to the pure system (Figure 7d). For $x_w \leq 0.3$ and $T \leq 7500$ K, the majority of O atoms have two Si nearest neighbors, but this majority is not as large as the four-coordinated Si atoms. As the overall mole fraction of water increases, f_{OSi_2} steadily decreases as f_{OSi_1} increases. This change is expected as the number of Si atoms present decreases as the mole fraction of water changes.

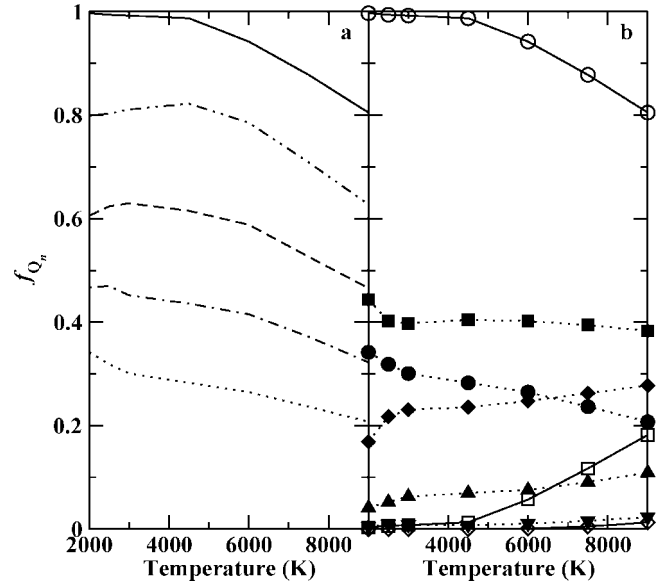

Figure 8. Fraction of Q_n populations as a function of temperature. (a) Fraction of Q_4 species for 0W (solid), 10W (dot-dot-dashed), 20W (dashed), 30W (dot-dashed), and 40W (dotted) compositions. (b) Fraction of Q_n for all n for 0W (open symbols) and 40W (closed symbols). Circles, squares, diamonds, triangles up, and triangles down indicate $n = 4$, 3, 2, 1, and 0, respectively. For the 0W composition, $n = 1$ and $n = 0$ are negligible and not shown.

One measure of the extended structure of the liquid is to examine the extent of the silica network. To this end, we use the Q_n notation employed in analyses of ^{29}Si NMR. In the following analysis, we will be examining only the tetrahedral Si environments, i.e. only those Si atoms bound to four O atoms, referred to as silica tetrahedra. The Q_n notation provides a means to compare the connectedness of the silica tetrahedra. The subscript n indicates the number of "bridging" O atoms, defined as O atoms with at least two Si nearest neighbors. No limits are put on the coordindation environment of these neighboring Si atoms. Thus, Q_0 is an isolated SiO_4 unit with no bridging O atoms whereas Q_4 is fully embedded in the silica network, with all four O atoms bridging to another Si atom. The relative populations of the Q_n species as a function of composition and temperature are shown in Figure 8. To simplify the comparison, only the Q_4 data is shown in Figure 8a for five compositions. For the pure silica system, Q_4 species are the most abundant over the entire temperature range. Even at 9000 K, 80% of the silica tetrahedra are fully coordinated to other Si atoms. The addition of even small amounts of water, as in the 10W system, disrupts the overall connectivity of the silica tetrahedra. For 10W, f_{Q_4} is 80% at 2000 K. This trend continues, almost linearly, with x_w. For 40W, Q_4 species account for no more than 35% of silica tetrahedra. These findings are in good agreement with the first principles simulations of Pöhlmann et al.[10] At $x_w = 0.118$, the fraction of Q_4 Si tetrahedra was found to be 74 ± 7% at 3000 K and 71 ± 6% at 3500 K, similar to the value of 78 ± 1% found here at $x_w = 0.117$ and $T = 3000$ K.

Figure 8b shows the two composition extremes, 0W and 40W. Here, each Q_n species that contributes ≥2% is shown. In neat silica, this includes only Q_2, Q_3, and Q_4 species, and the Q_3 species is found here to not exceed 20% even at 9000 K. In contrast, Q_3 is the major species at all temperatures for 40W. At higher temperatures, even Q_2 contributes to a larger fraction of silica tetrahedra than Q_4, with significant contributions from Q_1. The local silica tetrahedral network is disrupted more by the addition of water than by raising the temperature several thousand degrees.

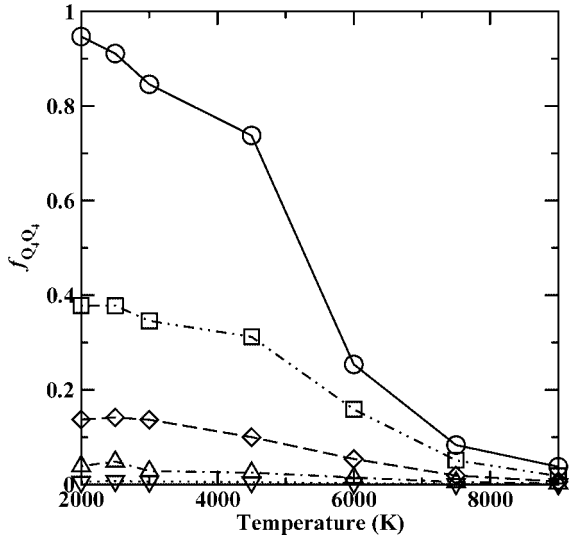

Figure 9. Fraction of Q_4 species corner-sharing with only Q_4 species as a function of temperature. The symbols are as follows: 0W (cirlces/ solid), 10W (squares/dot-dot-dashed), 20W (diamonds/ dashed), 30W (triangles up/dot-dashed), and 40W (triangles down/dotted) compositions.

TABLE 3: Analysis of Oxygen Atom Neighbor Environments for $x_w = 0.1$ as a Function of Temperature[a]

		f_{O_n} (%)					
total neighbors		2000 K	3000 K	4500 K	6000 K	7500 K	9000 K
0 neighbors		0.0	0.0	0.0	0.0	0.0	0.1_1
1 neighbor	1 Si	4.3_2	5.3_2	5.9_1	7.6_1	10.8_1	14.9_1
	1 H	0.1_1	0.0	0.0	0.0	0.1_1	0.11
2 neighbors	2 Si	89.7_2	89.9_3	89.6_1	83.2_1	74.5_1	68.1_1
	2 H	0.08_{17}	0.02_1	0.01_1	0.01_1	0.01_1	0.01_1
	1 Si, 1 H	5.7_3	3.9_1	2.5_2	1.9_3	1.8_1	1.8_2
3 neighbors	3 Si	0.0	0.5_2	1.4_1	6.3_1	11.5_1	13.5_1
	2 Si, 1 H	0.1_1	0.4_1	0.6_1	0.9_1	0.9_1	0.9_1
	1 Si, 2 H	0.01_1	0.02_1	0.03_1	0.02_1	0.02_1	0.02_1
>3 neighbors		0.0	0.0	0.01_1	0.13_1	0.39_1	0.63_4

[a] Standard error of the mean is given as subscript.

Looking more specifically at the Q_4 environments, Figure 9 shows the fraction of Q_4 tetrahedra that are corner-sharing with only other Q_4 tetrahedra ($f_{Q_4Q_4}$), i.e. each O atom bridges to another Q_4 Si tetrahedron. At 2000 K in pure silica, Q_4 species account for 99% of silica tetrahedra. Of these, 95% corner-share with only other Q_4 species. As the temperature increases, $f_{Q_4Q_4}$ steeply decreases to less than 10% at 9000 K, despite the fact that $f_{Q_4} \approx 0.8$. The other compositions show a similar steady decline as temperature increases, although each starts from a progressively lower fraction at 2000 K. For the 40W system, even at 2000 K, less than 1% of the Q_4 species neighbor only other Q_4 species. Thus, using the FG potential, hydrating a silica liquid, even to small degree, has a profound effect on the long-range tetrahedral silica network, while larger amounts of water are necessary to disrupt the local structure.

3.5. Speciation. One of the properties of great interest to those studying the role of water in silicate magmas is the speciation of water. Using particle-based simulation, the speciation of a system can be examined directly. Table 3 contains an analysis of the O-containing species present in these silica systems. This includes not only the Si−O species examined previously, but also the H-containing species. First, examining the 10W system as a function of temperature, the percentage of O atoms with two Si neighbors remains steady (≈90%) over the lower temperature range, 2000−4500 K, and then decreases significantly as the temperature increases further. The percentage of O atoms with one Si and one H neighbor decreases 3-fold from ≈6% to ≈2% from 2000 to 6000 K, but holds steady as T is further increased to 9000 K. At the same time, the percentages of O atoms with one neighbor (O1) and three neighbors (O3) increase sharply for $T > 4500$ K. The rise in O1 and O3 come from an increase in the fraction of O atoms with one and three Si neighbors, respectively. Evidence of these overcoordinated bridging O atoms was seen previously in the coordination environment analysis.

TABLE 4: Analysis of Oxygen Atom Neighbor Environments as a Function of Composition at 3000 K[a]

		f_{O_n} (%)				
total neighbors	0W	10W	20W	30W	40W	
0 neighbors		0.0	0.0	0.1_1	0.3_1	0.6_1
1 neighbor	1 Si	0.3_1	5.3_2	12.4_1	18.1_5	24.8_{41}
	1 H		0.0	0.4_1	1.7_2	3.02
2 neighbors	2 Si	96.4_3	89.9_3	78.6_1	67.5_3	54.7_{36}
	2 H		0.02_1	0.17_6	0.61_{17}	1.03_{18}
	1 Si, 1 H		3.9_1	7.8_1	11.4_2	15.5_3
3 neighbors	3 Si	3.3_3	0.5_2	0.2_1	0.1_1	0.1_1
	2 Si, 1 H		0.4_1	0.3_1	0.2_1	0.2_1
	1 Si, 2 H		0.02_1	0.0	0.09_1	0.13_1
>3 neighbors		0.0	0.0	0.0	0.0	0.0

[a] Standard error of the mean is given as subscript.

In Table 4, the same examination is performed over compositions at 3000 K, resulting in several pronounced trends. As the overall mole fraction of water increases, the fraction of O2 steadily decreases from 96 to 71%, while that of O1 increases from 0.3 to 28%. In contrast to the temperature analysis, there is no accompanying rise in O3. This, again, is in agreement with the previous analysis of the O−Si coordination environments (Figure 7). The overall decline in O2 is due to a significant, nearly linear, decrease in bridging O atoms as x_w increases, balanced in part by a rise in SiOH groups. Dangling SiO groups are the main source of O1 (25% for $x_w = 0.4$), although there is also a slight rise in the number of uncoordinated OH groups.

The simulations indicate that molecular water (an oxygen atom bound to two hydrogen atoms) is present only in very small amounts, e.g. the fractions of oxygen atoms belonging to a molecular water species are 0.2, 0.6, and 1.0% for systems 20W, 30W, and 40W, respectively, at 3000 K. Figure 10 highlights the fraction of oxygen atoms present as molecular water species as a function of temperature and composition. Overall, decreasing T and increasing x_w leads to an increase in molecular water. For $x_w < 0.22$ at all temperatures, fewer than 0.4% of oxygen atoms belong to a molecular water species. Using first principles simulations, Pöhlmann et al. found fractions of molecular water species of 0.06 and 0.3% at 3000 and 3500 K, respectively, for $x_w = 0.118$, although this includes "tethered" water molecules, where the O atom is bound to a Si atom in addition to two H atoms.[10] These species are not included in the fraction of molecular water shown in Figure 10. At the extreme, $T = 2000$ K and $x_w = 0.4$, molecular water accounts for 2.13% of oxygen atoms (or 0.25 wt %).

Under conditions ($T = 2000$ K and $x_w < 0.2$) most similar to those found within the Earth's mantle, the FG potential predicts that less than 0.4% of the oxygen atoms are part of free water molecules. Instead, water is dissociated and forms SiOH, dangling SiO, or free OH groups. To the authors' knowledge, the water speciation has not yet been probed

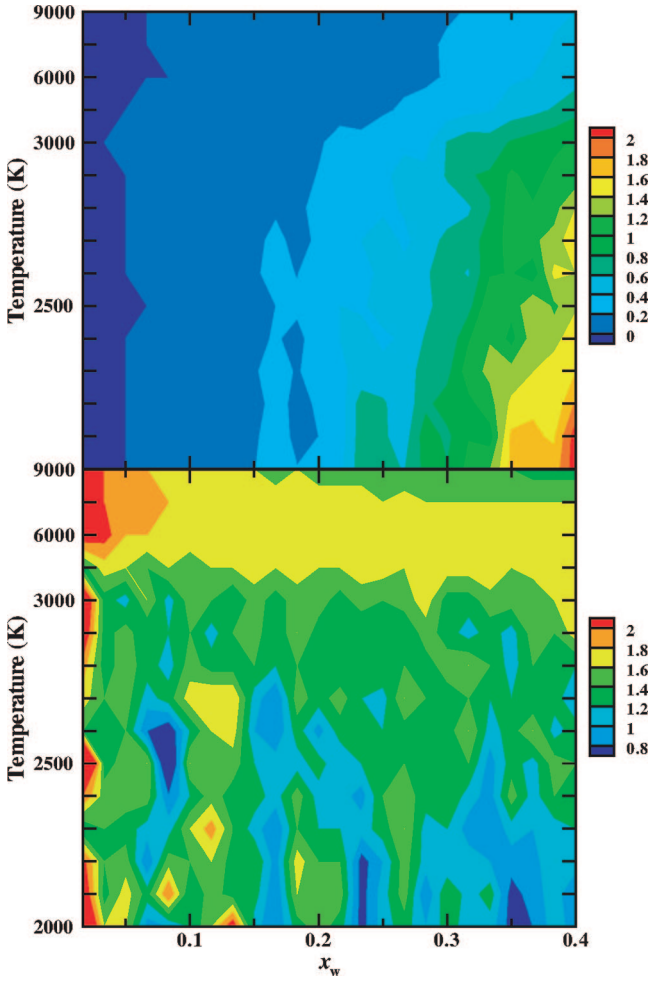

Figure 10. Percentage of oxygen atoms found as free water molecules (top) and natural logarithm of the apparent equilibrium constant (bottom) shown as functions of composition and temperature.

experimentally for hydrous silica melts at the temperatures investigated here. However, the speciation of silicate glasses has been extensively studied by spectroscopic techniques over a large temperature range.[3,4] In particular, the near-infrared combination bands at 4500 and 5200 cm^{-1} have been used to measure the concentrations of silanol groups and of molecular water, respectively.[27−30] The speciation is expressed in terms of the following equilibrium constant

$$K = [OH_{melt}]^2/([O_{melt}][H_2O_{melt}]) \quad (8)$$

where $[OH_{melt}]$, $[O_{melt}]$, and $[H_2O_{melt}]$ are the molar fractions of dangling hydroxyls, bridging oxygens, and molecular water in the melt, respectively, given in a single-oxygen basis. In the current simulations for hydrous silica melts at temperatures above 2000 K (and also the first principles simulations by Pöhlmann et al.[10]), additional types of oxygen environments are observed (see Tables 3 and 4). However, it should be noted that the concentration of under- and overcoordinated oxygen species is quite small below 3000 K and that the fraction of certain oxygen species is quite sensitive to the distance cutoff used (see discussion above). To enable a comparison with the experimental equilibrium constants (that only consider three different types of two-coordinated oxygen species), we searched for the two nearest atoms for every oxygen atom and grouped them into bridging oxygen (Si−O−Si), dangling hydroxyl (Si−O−H), molecular water (H−O−H), and three other environments that involve one or two oxygen atoms as nearest neighbors of the central oxygen. At 2000 and 3000 K, less than 0.1 and 0.5% of the oxygen atoms are found in the latter group of environments. However, as the temperature increases and the tetrahedral coordination of the melt starts to break down, the fraction of Si−O−O triads increases and reaches 14% at 9000 K. For the calculations of the equilibrium constants according to eq 8, we consider Si−O−O triads to belong to the bridging oxygen group.[31]

TABLE 5: Comparison of ln *K* Values from Simulations (x_w = 0.1) and Extrapolated from Spectroscopic Data for Hydrous Silicates[28–30] [a]

	2000 K	3000 K	4500 K	6000 K	7500 K	9000 K
simulation	1.2_8	1.5_2	1.5_1	1.7_1	1.7_1	1.7_1
LBZ-GG[b]	1.1_4	1.7_4	2.1_4	2.3_4	2.4_4	2.5_4
LBZ-TT[c]	0.2_2	0.6_2	0.9_2	1.1_2	1.1_2	1.2_2
NB-LB[d]	1.2_2	1.9_2	2.4_2	2.6_2	2.8_2	2.9_2

[a] Standard error of the mean is given as subscript. [b] Reference 30; dacitic melt; T = 753−863 K, p = 100 kPa, using two Gaussian curves to fit baseline, ln K = 2.88−3567/T. [c] Reference 30; dacitic melt; T = 753−863 K, p = 100 kPa, using two tangential lines to fit baseline, ln K = 1.49−2634/T. [d] Reference 28; rhyolitic melt; T = 773−1073 K, p = 100−300 MPa, using linear baseline, ln K = 3.33−4210/T.

The natural logarithm of the equilibrium constants calculated in this manner for system 10W are compared in Table 5 to extrapolated equilibrium constants obtained from fits to experimental data for dacitic and rhyolitic melts with total water concentrations of about 2.5 wt % at temperatures up to 1073 K.[28,30] At the lower temperatures, the statistical uncertainties for ln K obtained from the five independent simulations for system 10W are quite large, that is, even for an empirical potential it is difficult to reach simulation lengths that yield well-converged species distributions. The extrapolations of the experimental data give ln k values from 0.2 to 1.2 at 2000 K and from 1.2 to 2.9 at 9000 K,[28,30] and over the entire temperature range, the simulation data fall within the range of these extrapolations. Recent first principles simulations[32] of a hydrous $MgSiO_3$ melt at 3000 K and near-ambient pressure indicated ln $K \approx 1.1$, i.e. a value within the range of the extrapolations and close to the value of 1.5 obtained for the FG potential.

The temperature and composition dependence of ln K for the simulations is graphically depicted in Figure 10. As can be seen, larger values of ln K are found at higher temperature and lower x_w. The state point dependence of ln K is less pronounced (and shows more scatter) than that for the fraction of molecular water species and, since the concentration of molecular water appears as reactant in the chemical equilibrium represented by eq 8, small values of ln K correspond to large fractions of molecular water. Overall, the speciation found for the FG potential qualitatively agrees with spectroscopic analysis of H_2O-rich silicate glasses that commonly indicate a small proportion of molecular water species (extrapolated to T > 2000 K) and that the formation of molecular water is favored at low temperatures and high total H_2O contents.[28−30]

3.6. System Size Effects. We recognize that the results discussed so far are based on simulations for a relatively small system size, 180 atoms. In an effort to validate the previous results, we ran simulations of the five main compositions for systems consisting of 720 and 1440 atoms (240 and 480 formula units, respectively) at 3000 and 6000 K. For each composition, five independent simulations were performed. Apart from system

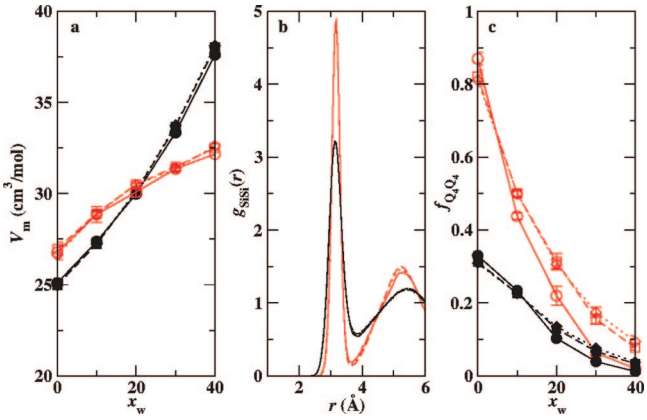

Figure 11. System size effects on (a) molar volume, (b) Si−Si radial distribution function, and (c) $f_{Q_4Q_4}$. Circles (solid lines), squares (dashed lines), and diamonds (dotted lines) indicate 180, 720, and 1440 atoms, respectively, at 3000 (red) and 6000 K (black). For the RDF, only the 10W system is shown.

TABLE 6: System Size Effects on the Fraction of O2 species[a]

	f_{O_2} (%)								
	0W			20W			40W		
system size	180	720	1440	180	720	1440	180	720	1440
				3000 K					
2 Si	96.4_3	96.2_5	95.9_3	78.6_1	79.1_2	79.0_2	54.5_4	55.8_5	55.2_3
2 H				0.2_1	0.2_1	0.2_1	1.0_1	1.3_1	1.2_1
1 Si, 1 H				7.8_1	7.6_1	7.5_1	15.5_3	14.6_3	15.3_2
				6000 K					
2 Si	84.9_1	84.2_1	84.2_1	74.1_1	73.3_2	73.4_1	51.6_1	51.6_1	51.4_1
2 H				0.1_1	0.1_1	0.1_1	0.5_1	0.6_1	0.6_1
1 Si, 1 H				4.8_1	4.8_1	4.7_1	11.0_1	10.8_1	10.8_1

[a] Standard error of the mean is given as subscript.

size, all other conditions were kept the same. Selected results from these simulations are presented in Figure 11.

First, we consider the molar volume of the system (Figure 11a). For 6000 K, the molar volume of the system for each composition is the same, within the error bars, for each system size. At the lower temperature, the molar volume for the small system size is slightly smaller than the large systems, but this difference is less than 1.5%.

Second, Figure 11b shows the Si−Si RDF for each system size for 10W. At 3000 K, there are no significant structural changes between the systems. For the higher temperature, the height of the second peak increases slightly with increasing number of atoms in the system.

Third, we examined the effect of system size on $f_{Q_4Q_4}$ (Figure 11c). Here, the system-size effect is greatest. At 3000 K, the small system underestimates $f_{Q_4Q_4}$ by as much as 75% for 40W as compared to the largest system. For 0W, $f_{Q_4Q_4}$ is overestimated by 10%. Similar trends are apparent at the higher temperature as well, although not as dramatic. The fraction of Q_4 species with only Q_4 species is a third nearest Si neighbor effect. In the small system, the third nearest Si neighbor of a given Si atom may be more than half of the box length away.

Finally, the system size effect on the speciation is indicated in Table 6 for O2 species. In general, the system size effects on speciation are quite small. At 3000 K, slightly more molecular water species are found for the larger systems at $x_w = 0.4$. At 6000 K, the smallest system tends to overpredict slightly for bridging O species (2 Si neighbors) for compositions 0W and 20W.

4. Conclusions

We examined the structural behavior of hydrated liquid silica as a function of temperature and composition. Pure liquid silica modeled with the Feuston−Garofalini potential exhibits a volume minimum near 7650 K. With the addition of water, the temperature of the volume minimum decreases and, for $x_w > 0.267$, disappears. The minimum arises from changes in the silica structure as a function of temperature. The predominantly tetrahedral silica network is compressed within the volume depression region, leading to overcoordination of both Si and O atoms. This is primarily a local effect, seen in the number integral of Si−Si and O−O as well as the coordination number of O around Si and Si around O. Long range structure, as indicated by $f_{Q_4Q_4}$, shows a dramatic decrease in corner-sharing Q_4 tetrahedra as the temperature increases. In the hydrated systems, low water concentration systems, $x_w < 0.2$, show local structure very similar to the pure system, while long-range structure is disrupted by even small concentrations of water ($x_w \geq 0.1$). As x_w increases, disruptions occur not only in the long-range structure, but the local environments of the Si and O atoms change as well. For all compostions and temperatures, less than 2.5% of O atoms are present as molecular water, i.e. are bound to two H atoms. Using the FG potential, it is clear that molecular water dissociates to form SiOH, Si_2O, and unbound OH groups at $p = 1$ GPa and $T \geq 2000$ K. Finally, additional simulations using other reactive force fields and density functional theory are needed to assess the validity of the observations reported here for the FG potential.

Acknowledgment. Financial support was provided by the National Science Foundation (ITR-0428774) and the 3M Science and Technology and Louise Dosdall Fellowships (K.E.A.). Computer resources were provided by the Minnesota Supercomputing Institute.

References and Notes

(1) Poirier, J. P. *Intorduction to the Physics of the Earth's Interior*, 2nd ed.; Cambridge University Press: Cambridge, 2000.
(2) Lange, R. A. *Rev. Mineral.* **1994**, *30*, 331.
(3) McMillan, P. F. *Rev. Mineral.* **1994**, *30*, 131.
(4) Kohn, S. C. *Mineral. Mag.* **2000**, *64*, 389.
(5) Sarnthein, J.; Pasquarello, A.; Car, R. *Phys. Rev. Lett.* **1995**, *74*, 4682.
(6) Sarnthein, J.; Pasquarello, A.; Car, R. *Phys. Rev. B* **1995**, *52*, 12690.
(7) Benoit, M.; Ispas, S.; Tuckerman, M. E. *Phys. Rev. B* **2001**, *64*, 224205.
(8) Trave, A.; Tangney, P.; Scandolo, S.; Pasquarello, A.; Car, R. *Phys. Rev. Lett.* **2002**, *89*, 245504.
(9) Karki, B. B.; Bhattarai, D.; Stixrude, L. *Phys. Rev. B* **2007**, *76*, 104205.
(10) Pöhlmann, M.; Benoit, M.; Kob, W. *Phys. Rev. B* **2004**, *70*, 184209.e.
(11) Feuston, B. P.; Garofalini, S. H. *J. Phys. Chem.* **1990**, *94*, 5351.
(12) Litton, D. A.; Garofalini, S. H. *J. Appl. Phys.* **2001**, *89*, 6013.
(13) Rustad, J. R.; Hay, B. P. *Geochim. Cosmochim. Acta* **1995**, *59*, 1251.
(14) Rustad, J. R.; Wasserman, E.; Felmy, A. R.; Wilke, C. *J. Colloid Interface Sci.* **1998**, *198*, 119.
(15) van Duin, A. C. T.; Dasgupta, S.; Lorant, F.; Goddard, W. A. *J. Phys. Chem. A* **2001**, *105*, 9396.
(16) van Duin, A. C. T.; Strachan, A.; Stewman, S.; Zhang, Q.; Xu, X.; Goddard, W. A. *J. Phys. Chem. A* **2003**, *107*, 3803.
(17) Kuzuu, N.; Yoshie, H.; Tamai, Y.; Wang, C. *J. Non-Cryst. Solids* **2004**, *349*, 319.
(18) Anderson, K. E.; Grauvilardell, L. C.; Hirschmann, M. C.; Siepmann, J. I. *J. Phys. Chem. B* **2008**, *112*, 13015.
(19) Stillinger, F. H.; Rahman, A. *J. Chem. Phys.* **1978**, *68*, 666.
(20) Rao, N. Z.; Gelb, L. D. *J. Phys. Chem. B* **2004**, *108*, 12418.
(21) Stillinger, F. H.; Weber, T. A. *Phys. Rev. B* **1985**, *31*, 5262.
(22) McDonald, I. R. *Mol. Phys.* **1972**, *23*, 41.
(23) Hudon, P.; Jung, I.-H.; Baker, D. H. *Phys. Earth Planet. Mater.* **2002**, *130*, 159.

(24) Brückner, R. *J. Non-Cryst. Solids* **1970**, *5*, 123; Brückner, R. *J. Non-Cryst. Solids* **1971**, *5*, 281.
(25) Ochs, F. A.; Lange, R. A. *Contrib. Mineral Pet.* **1997**, *129*, 155.
(26) Lange, R. A.; Carmichael, I. S. E. In *Reviews in Mineralogy: Modern Methods of Igneous Petrology*; Nicholls, J., Russell, K., Eds.; Mineralogical Society of America: Washington, 1990; Vol. 24, pp 25−64.
(27) Withers, A. C.; Behrens, H. *Phys. Chem. Minerals* **1999**, *27*, 199.
(28) Novak, M.; Behrens, H. *Earth Planet. Sci. Lett.* **2001**, *184*, 515.
(29) Behrens, H.; Novak, M. *Phase Trans.* **2003**, *76*, 45.
(30) Liu, Y.; Behrens, H.; Zhang, Y. X. *Am. Mineral.* **2004**, *89*, 277.
(31) Alternatively, the equilibrium constants were also calculated using the oxygen species listed in Table 3. In this case, it was assumed that oxygen atoms that are connected to 1 H atom and 1 or 2 Si atoms contribute to $[OH_{melt}]$, that oxygen atoms that are connected to 2 H atoms and 0 or 1 Si atom contribute to $[H_2O_{melt}]$, and that all other oxygen species (including isolated hydroxide fragments) do not contribute to either the peak at 4500 or 5200 cm^{-1} and hence are part of $[O_{melt}]$. Using this approach, $\ln K = 1.3 \pm 1.0$ and 1.5 ± 0.5 for system 10W at 2000 and 3000 K, respectively. However, at higher temperatures, the $\ln K$ values are more scattered and are generally lower than those found by searching for the two nearest-neighbor atoms of each oxygen atom.

(32) Mookherjee, M.; Stixrude, L.; Karki, B. *Nature* **2008**, *452*, 983.

JP802253D